

Study of B1 (NaCl-type) to B2 (CsCl-type) pressure-induced structural phase transition in BaS, BaSe and BaTe using *ab initio* computations

This article has been downloaded from IOPscience. Please scroll down to see the full text article.

2013 J. Phys.: Condens. Matter 25 075401

(<http://iopscience.iop.org/0953-8984/25/7/075401>)

View [the table of contents for this issue](#), or go to the [journal homepage](#) for more

Download details:

IP Address: 131.183.160.228

The article was downloaded on 23/01/2013 at 17:21

Please note that [terms and conditions apply](#).

# Study of B1 (NaCl-type) to B2 (CsCl-type) pressure-induced structural phase transition in BaS, BaSe and BaTe using *ab initio* computations

X Zhou<sup>1</sup>, J L Roehl<sup>2</sup>, C Lind<sup>1</sup> and S V Khare<sup>2</sup>

<sup>1</sup> Department of Chemistry, The University of Toledo, 2801 West Bancroft Street, Toledo, OH 43606, USA

<sup>2</sup> Department of Physics and Astronomy, The University of Toledo, 2801 West Bancroft Street, Toledo, OH 43606, USA

E-mail: [sanjay.khare@utoledo.edu](mailto:sanjay.khare@utoledo.edu)

Received 17 October 2012, in final form 6 December 2012

Published 22 January 2013

Online at [stacks.iop.org/JPhysCM/25/075401](http://stacks.iop.org/JPhysCM/25/075401)

## Abstract

We have studied the pressure-induced phase transitions from NaCl-type (B1) to CsCl-type (B2) structure in BaS, BaSe and BaTe by using *ab initio* density functional theory computations in the local density approximation. The Buerger and WTM mechanisms were explored by mapping the enthalpy contours in two- and four-dimensional configuration space for the two mechanisms, respectively. Transition pressures for BaS, BaSe and BaTe were determined to be 5.5 GPa, 4.9 GPa and 3.4 GPa, respectively. From these configuration space landscapes, a low enthalpy barrier path was constructed for the transitions to proceed at three different pressures. We obtained barriers of 0.18, 0.16 and 0.15 eV/pair (17.4, 15.4 and 14.6 kJ mol<sup>-1</sup>) for the Buerger mechanism and 0.13, 0.13 and 0.12 eV/pair (12.5, 12.5 and 11.6 kJ mol<sup>-1</sup>) for the WTM mechanism at the transition pressures for BaS, BaSe and BaTe, respectively, indicating that the WTM mechanism is slightly more favorable in these compounds. We describe the difference between the two mechanisms by differences in their symmetry and atomic coordination.

(Some figures may appear in colour only in the online journal)

## 1. Introduction

Possible mechanisms of phase transition of binary compounds from the six-coordinated B1 structure (NaCl-type,  $Fm\bar{3}m$ ) to the eight-coordinated B2 structure (CsCl-type,  $Pm\bar{3}m$ ) have been studied both experimentally and theoretically over the past decades [1–8]. Two transition mechanisms are generally discussed in this type of phase transition. Buerger proposed the first mechanism, in which the angle of a rhombohedral primitive cell with the B1 structure increases from 60° to 90° and results in the B2 structure [1]. Watanabe *et al* [2] discussed a second possibility, referred to as the WTM mechanism, based on their x-ray studies and optical observations on the phase transition of CsCl. In this mechanism, the phase transition from the B1

to the B2 structure involves a translational displacement between two adjacent layers of atoms. Stoke and Hatch [3] studied all the common subgroups of the B1 and B2 structures for more possibilities. They suggested that a third mechanism, the  $P2_1/m$  mechanism, should be considered when an intermediate phase is observed on the transition pathway, though the Buerger and WTM mechanism are more energetically favorable. Toledano *et al* [9] suggested another mechanism, where the B1/intermediate/B2 transitions are described in space groups  $Pnma$  and  $Pbcm$ . Both the  $P2_1/m$  and Toledano pathways provide good explanations for the B1 to B2 phase transitions with intermediate states [9, 10]. While several theoretical investigations on the transition mechanisms have been published, only a few papers have

characterized the transition mechanisms by modeling their energy hypersurfaces [5, 6].

The barium chalcogenides BaX (X = S, Se and Te), henceforth referred to as BaX when all three compounds are involved, are potential materials for light-emitting diodes and laser diodes [11]. They exhibit reversible pressure-induced phase transitions from the B1 to the B2 phase at moderate pressures (4.8–6.5 GPa) [12–14]. No intermediate phase has been observed during the transition. A phase space region of BaS was reported by Yamaoka *et al* [12], where the two phases coexisted above or below the transition pressure during the pressure increase or release, respectively. With further application of pressure, the B2 phases of BaX are stable until their metallization pressures of about 80, 52 and 20 GPa, for X = S, Se and Te, respectively [14–16].

In this paper, we present a density functional theory (DFT) based *ab initio* computational study on the Buerger and WTM mechanisms for BaX. There has been no experimental observation of any intermediate phase for the B1–B2 phase transition of BaX. Hence, the  $P2_1/m$  and Toledano pathways are not studied in our work. Many theoretical investigations on the pressure-induced phase transitions of barium chalcogenides have focused on obtaining the transition pressure, band structure, density of states and elastic properties [11, 17–21]. The study of the energy hypersurfaces and resulting pathways for the transition with the two competing mechanisms has been left unexplored. In this work, we report such a study of the energy hypersurfaces of BaX at pressures above, at, and below the transition pressure. Transition paths and energy barriers of the two different mechanisms are compared. Structural changes along the transition path are described. Our results are compared with earlier experimental and theoretical work. Pendas *et al* [5] mentioned that it could be difficult to study the transition dynamics and kinetics experimentally due to impurities, defects, thermal and mechanical history and experimental parameters. In addition, nucleation processes can have a profound influence on the pressure-induced B1–B2 phase transition, and the transition may not be purely homogeneous [22, 23]. However, by using idealized theoretical models for both the Buerger and WTM mechanisms, the microscopic lattice dynamics of the two different transition mechanisms can be predicted and compared. Therefore, our work can further elucidate the transition mechanisms from the B1 to the B2 structure. Section 2 describes the Buerger and WTM mechanisms for the B1 to B2 structural transition; section 3 describes our computational method; section 4 describes the modeling approach; section 5 describes and discusses our results and section 6 gives the conclusions.

## 2. Transition mechanisms

The Buerger mechanism [1] (mechanism I) and WTM mechanism [2] (mechanism II), shown in figure 1, can be characterized in one of the two common subgroups of the B1 and B2 structures,  $R\bar{3}m$  and  $Pm\bar{3}n$ , respectively [6].

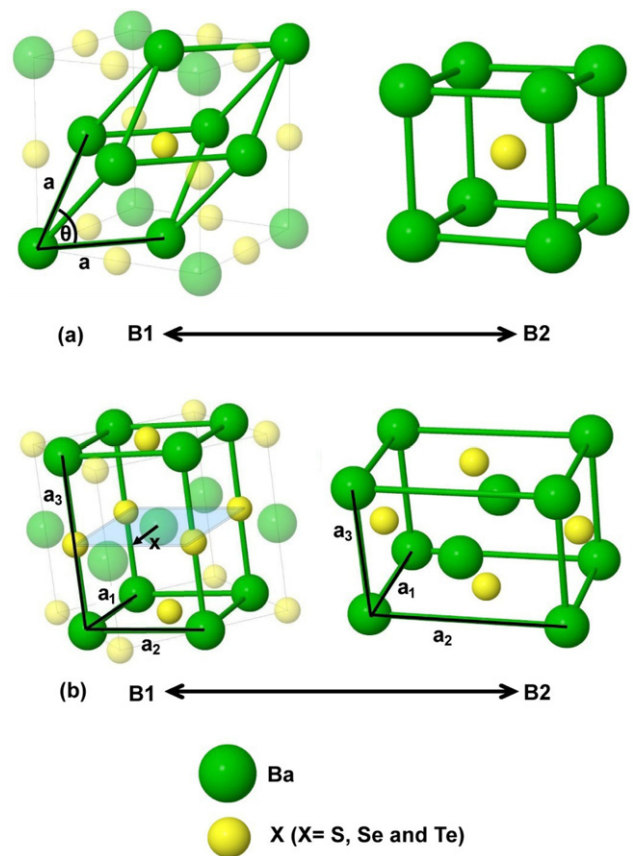


**Figure 1.** The transition from the B1 to the B2 structure depicted in (a) rhombohedral unit cell (used for mechanism I) and (b) orthorhombic unit cell (used for mechanism II). Mechanism I is the Buerger mechanism, in which the rhombohedral cell with a space group of  $R\bar{3}m$  is compressed along its diagonal and results in a transformation to the B2 structure. The variables in the transition for mechanism I are the angle ( $\theta$ ) between two cell edges and lattice constant  $a$  of the unit cell. Mechanism II is the WTM mechanism, in which atoms in the (002) plane of the orthorhombic unit cell, with a space group of  $Pm\bar{3}n$  translate by half a lattice vector ( $\vec{a}_1/2$ ) causing a transformation to the B2 structure. The variables in this transition are the lattice constants  $a$ ,  $b$  and  $c$ , which are the magnitude of lattice vectors  $\vec{a}_1$ ,  $\vec{a}_2$ , and  $\vec{a}_3$ , respectively and the internal parameter  $x$ , which is the ratio between the distance that the atoms in the (002) plane have moved and the magnitude of the lattice vector  $\vec{a}_1$ . The limiting values of  $x$  are 0 and 0.5 for B1 and B2 structures while those of  $\theta$  are  $60^\circ$  and  $90^\circ$ , respectively.

For BaX in mechanism I, the B1 and B2 structures can be represented by a two-atom rhombohedral primitive cell, with the Ba and X atoms on the corners and centers of the unit cell, respectively. The cell is defined by the magnitude ‘ $a$ ’ of each lattice vector and the angle  $\theta$  between any two of them. Thus  $a$  and  $\theta$  are the only two variables in mechanism I. When  $\theta = 60^\circ$ , the two-atom rhombohedral cell when extended through all space becomes isomorphic with an eight-atom face-centered cubic cell, which is the B1 structure. When  $\theta = 90^\circ$ , the rhombohedral cell becomes a primitive cubic cell, which is the B2 structure. During the pressure-induced phase transition from the B1 to the B2 structure, the rhombohedral unit cell is compressed along its body diagonal, which results

in a decrease of the unit cell lattice constant  $a$ , accompanied with an opening of the angle  $\theta$  from  $60^\circ$  to  $90^\circ$ .

In mechanism II, the B1 and B2 structures can be represented by a four-atom orthorhombic unit cell with three orthogonal lattice vectors ( $\vec{a}_1$ ,  $\vec{a}_2$ , and  $\vec{a}_3$ ), and an internal parameter ' $x$ '. For the B1 structure, the positions for the two Ba atoms are the corners and the body center of the unit cell. Two X atoms are located on two opposing face centers, which are perpendicular to the vector  $\vec{a}_3$ . Four additional X atoms lie on centers of the four edges parallel to the vector  $\vec{a}_3$ . During the pressure-induced phase transition from the B1 to the B2 structure, atoms on the (002) plane of BaX slide along the [100] direction. The resulting relative displacement is called the internal parameter  $x$ . It is defined as the ratio of the magnitudes of the displacement of the moving atoms and that of the lattice vector  $\vec{a}_1$ . When the transition is complete, the Ba atoms that occupy the body centers of the B1 structure are located on the face centers of the (100) planes of the B2 structure, while the X atoms are moved from their positions in the B1 structure to the face-centered sites of the (010) planes. Therefore,  $x$  increases from 0 to 0.5 as the transition goes from the B1 to the B2 phase. The phase transition of mechanism II is characterized by the lattice constants  $a$ ,  $b$  and  $c$ , which are the magnitudes of the lattice vectors  $\vec{a}_1$ ,  $\vec{a}_2$ , and  $\vec{a}_3$ , respectively, and the internal parameter  $x$ . Because of geometric constraints, the relations between  $a$ ,  $b$  and  $c$  are  $\sqrt{2}a = \sqrt{2}b = c$  and  $\sqrt{2}a = b = c$  for the B1 and B2 structures, respectively.

### 3. Computational method

All the *ab initio* calculations in this work are performed by using the Vienna *ab initio* simulation package (VASP) [24–27] codes within the local density approximation (LDA) to density functional theory (DFT) [28, 29]. The electron–ion interactions are treated by ultrasoft-Vanderbilt type pseudo-potentials [30] as supplied by Kresse *et al* [31]. Three cutoff energies, 210 eV, 170 eV and 140 eV, are applied to the valance electronic wave functions expanded in a plane-wave basis set for BaS, BaSe and BaTe, respectively. A Monkhorst–Pack [32] generated  $6 \times 6 \times 6$   $k$ -point grid was used for the Brillouin-zone integrations in all calculations with both mechanism I and mechanism II. Tests using cutoff energies and  $k$ -points mentioned above reached a convergence better than 1 meV. The minimum energy for each configuration with the B1 or the B2 structure at a certain pressure was obtained by fully relaxing all atoms and lattice constants until a force convergence to less than  $0.01 \text{ eV } \text{\AA}^{-1}$  was achieved. In order to fully explore the lattice space of the four-dimensional (4D) orthorhombic unit cells in the WTM mechanism, more than 200 000 structure configurations were constructed.

### 4. Modeling approach

The potential energy surface (PES) [5, 33] is approached by obtaining enthalpy as a function of structural parameters,

which can be described as  $H_I = H_I(\theta, a)$  and  $H_{II} = H_{II}(x, a, b, c)$  for mechanism I and mechanism II, respectively. Because  $H = U + PV$ , where  $U$  is internal energy,  $P$  is pressure and  $V$  is volume, each value of the enthalpy in these energy hypersurfaces was obtained by combining the computed value of the total energy ( $U$ ) of each structure with the product of the pressure and volume of the corresponding unit cell.

Since the energy hypersurfaces of mechanism I are two-dimensional (2D), the phase transition can be completely characterized by the two variables  $\theta$  and  $a$ , which determine the size and shape of the rhombohedral primitive cell. For mechanism I, each PES of a fixed pressure was computed for 13 uniformly distributed values of  $\theta$  between  $57^\circ$  and  $93^\circ$ . For each value of  $\theta$ , 12–14 values for the variable  $a$  were chosen from about  $0.1 \text{ \AA}$  below the lattice constant  $a$  of the B2 structure to about  $0.1 \text{ \AA}$  above the lattice constant  $a$  of the B1 structure. The three lattice vectors of mechanism I are defined by:

$$\vec{a}_i \cdot \hat{e}_j = (m + \delta_{ij}) \cdot d_m \quad (i, j = 1, 2 \text{ and } 3)$$

where  $\hat{e}_j$  are unit vectors along the Cartesian axes,  $\delta_{ij}$  is the Kronecker delta function,  $m \equiv (\sqrt{(1 + 2 \cos \theta)/(1 - \cos \theta)} - 1)/3$ ,  $d_m \equiv a \cdot (3m^2 + 2m + 1)^{-1/2}$ , and the corresponding position vectors for each atom are defined by:

$$\vec{b}_{Ba}^I = (0, 0, 0), \quad \vec{b}_S^I = (0.5, 0.5, 0.5),$$

in relative coordinates. The energy hypersurfaces in mechanism II are 4D, which would involve building a 4D grid. This would require prohibitive computational time. Therefore, instead of 4D energy hypersurfaces, we constructed 2D PES with  $x$  and  $c$  as independent variables and  $a$  and  $b$  as the dependent ones. For each fixed  $x$  and  $c$ , the enthalpy is minimized by finding the minimum value of a computed 2D enthalpy contour of  $11 \times 11$  mesh grids with  $a$  and  $b$  as variables. Each PES of a fixed pressure was computed for 11 uniformly distributed values of  $x$  between 0 and 0.5. For each value of  $x$ , 12–14 values for the variable  $c$  were chosen from about  $0.1 \text{ \AA}$  below the lattice constant  $c$  of the B2 structure to about  $0.1 \text{ \AA}$  above the lattice constant  $a$  of the B1 structure. The three lattice vectors of mechanism II are  $\vec{a}_1 = (a, 0, 0)$ ,  $\vec{a}_2 = (0, b, 0)$ , and  $\vec{a}_3 = (0, 0, c)$ , and the corresponding position vectors for each atom in relative coordinates are:

$$\begin{aligned} \vec{b}_{Ba1}^{II} &= (0, 0, 0), & \vec{b}_{Ba2}^{II} &= (0.5 - x, 0.5, 0.5), \\ \vec{b}_{S1}^{II} &= (0.5, 0.5, 0), & \vec{b}_{S2}^{II} &= (1 - x, 0, 0.5). \end{aligned}$$

The transition path from the B1 structure to the B2 structure is defined by connecting the points on the energy hypersurface that minimize the enthalpy. Starting at the initial B1 structure, the transition path connects points that result in the minimum increase of enthalpy up to the point that enthalpy starts to decrease. At this point, the transition path connects points that result in the maximum decrease of enthalpy to the final B2 structure. The transition energy barriers are obtained by finding the maximum enthalpy elevation on the transition

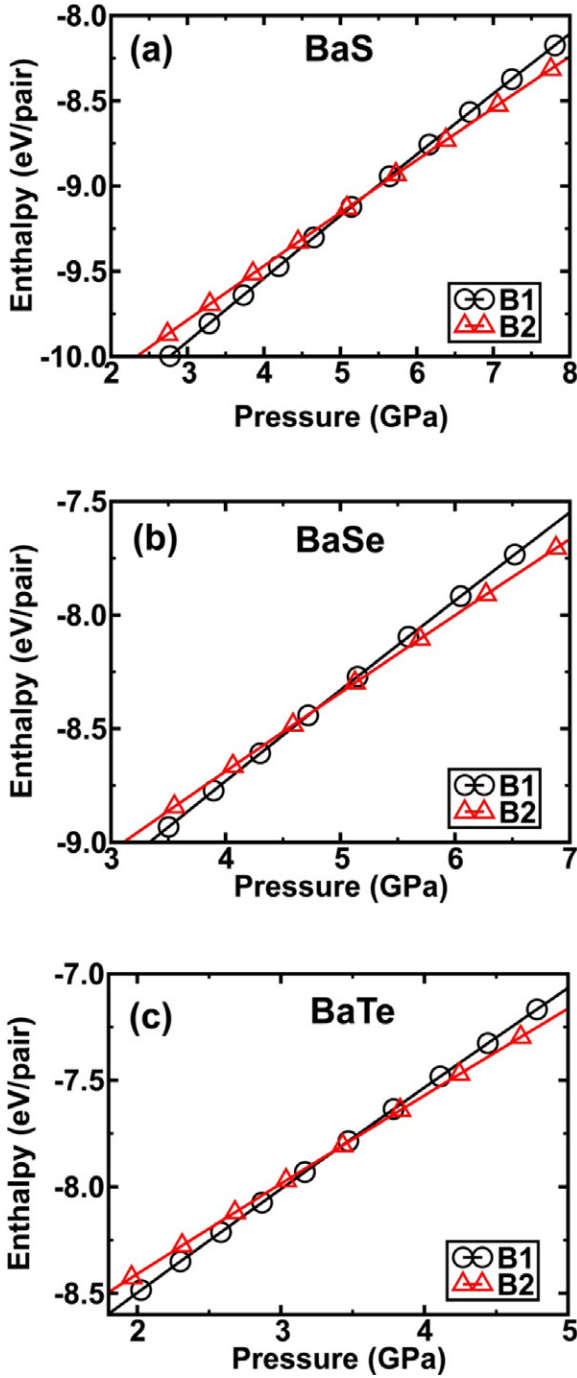


**Figure 2.** Plots of enthalpy (eV/pair) of one pair of atoms as a function of pressure (GPa) of (a) BaS, (b) BaSe, and (c) BaTe. Circles and triangles indicate computed data points of the enthalpy–pressure line of B1 and B2 structures respectively. Linear fits are made to these points and transition pressures are calculated at the intersections of these lines at 5.47 GPa, 4.87 GPa and 3.42 GPa for BaS, BaSe and BaTe, respectively.

path from the B1 to the B2 structure. In order to obtain accurate values of transition energy barriers, hypersurfaces of the surroundings of the saddle points with denser mesh grids are obtained. A convergence of 1 meV is achieved for each consecutive step on the transition path in the high resolution region.

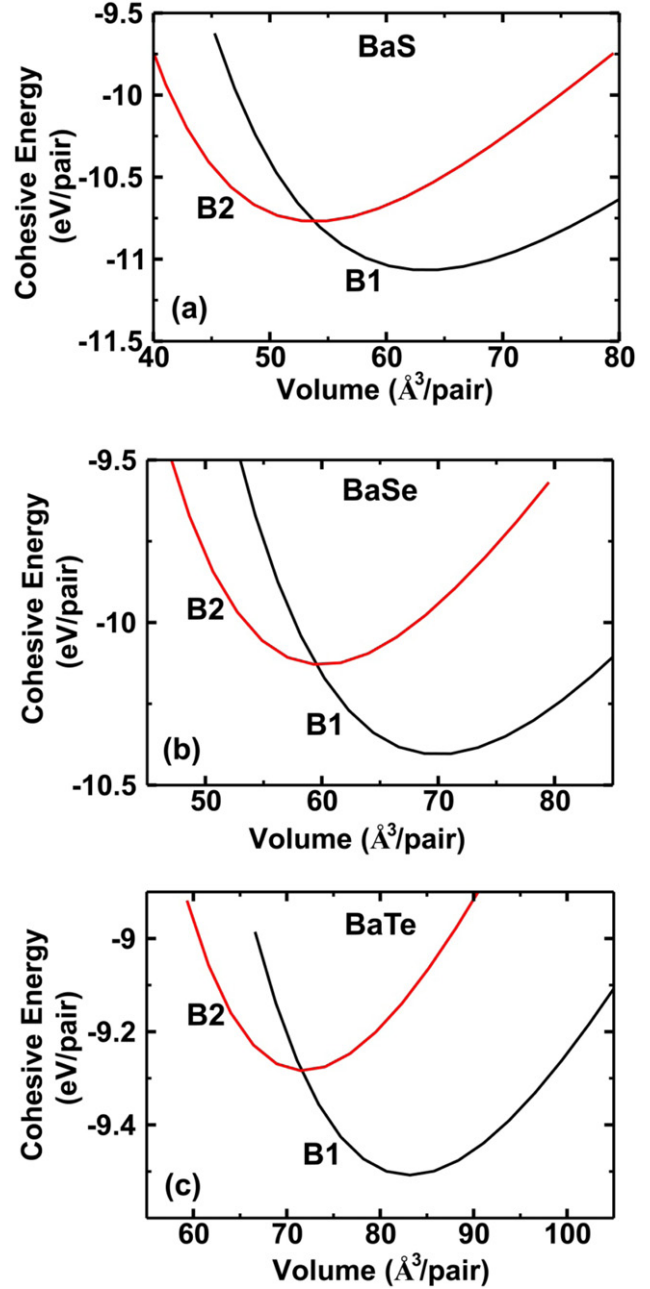


**Figure 3.** Plots of cohesive energy (eV/pair) of one pair of atoms as a function of volume (Å<sup>3</sup>/pair) of (a) BaS, (b) BaSe, and (c) BaTe for B1 and B2 structures.

## 5. Results and discussion

### 5.1. Transition pressure and structural parameters

At the transition pressure ( $P_t$ ) of BaX ( $X = S, Se$  and  $Te$ ), the enthalpy of the B1 structure is equal to that of the B2 structure. Therefore, the transition pressure can be calculated by solving the roots of the fitted linear equations of enthalpy as a function of pressure of the B1 and B2 structures. Figure 2 shows the plots of enthalpy (eV/pair) versus pressure (GPa) for all BaX, and the corresponding energy (eV/pair) versus volume plots are shown in figure 3 for comparison. For

each material, linear regression fits to the data points of the respective enthalpy–pressure lines of the B1 and B2 phases give the coefficient of determination  $R^2$  values of 0.999. For BaS, BaSe and BaTe the computed transition pressures are 5.47 GPa, 4.87 GPa and 3.42 GPa, respectively.

The values of the calculated  $P_t$ , as well as other structural parameters, are compared with experimental and theoretical data in table 1. The agreement between our results and other experimental and theoretical results is reasonable considering the differences in different computational methods as well as the experimental conditions used.

We found that the B1 phase of all BaX compounds exhibits lower cohesive energy ( $U$ ) than the corresponding B2 phase at zero pressure and therefore results in lower enthalpy, which explains why the B1 structure is the thermodynamically stable phase in nature at low temperature and pressure [12–14]. With increasing pressure, the cohesive energy of the B1 phase remains lower than that of the B2 phase. However, the difference in enthalpy ( $H_I^{B1} - H_I^{B2}$ ) between the enthalpies of the B1 and B2 phases becomes smaller. This is because the B1 structure exhibits a much larger volume than the B2 structure at the same pressure, causing the  $PV$  term to become important. As an example, the specific volumes of the B1 and B2 phases at the respective transition pressures are 57.8 and 49.4  $\text{\AA}^3/\text{pair}$  for BaS, 63.3 and 54.6  $\text{\AA}^3/\text{pair}$  for BaSe, and 76.4 and 66.4  $\text{\AA}^3/\text{pair}$  for BaTe. When the pressure increases so that  $P \geq P_t$ , the B1 phase is no longer energetically favorable, and the phase transition to the B2 phase occurs, which results in a significant reduction in volume and increase in coordination number. Our calculations are consistent with experimental observations [12–14].

### 5.2. Potential energy surface and energy barriers

The potential energy surfaces (PES) of BaS at 0, 5.5 and 8.0 GPa, BaSe at 0, 4.9 and 8.0 GPa, and BaTe at 0, 3.4 and 5.5 GPa for both mechanisms were computed. The PES at different pressures for a given material with a fixed mechanism are very similar. Hence only the PES plots at the transition pressure are shown in figures 4 and 5, for mechanism I and mechanism II, respectively. The color bar indicates the enthalpy difference between a specific structure and the B1 structure of the material at the corresponding pressure. Two minima corresponding to the B1 and B2 structures, whose enthalpies are equal at the transition pressure, are found on each PES plot. The dotted line on each PES plot indicates the computed transition pathway, whose cubic order polynomial fit is given in table 2, from the B1 to the B2 structure.

For mechanism I, there are only two variables, the angle  $\theta$  and the lattice constant  $a$ , represented by the  $x$  and  $y$  axes on the contours, respectively. From figure 4, only one transition pathway, whose shape is very close to the diagonal on the PES, is found possible for each material. These transition pathways suggest that both the angle and lattice constant change proportionately and simultaneously during the phase transition in mechanism I.

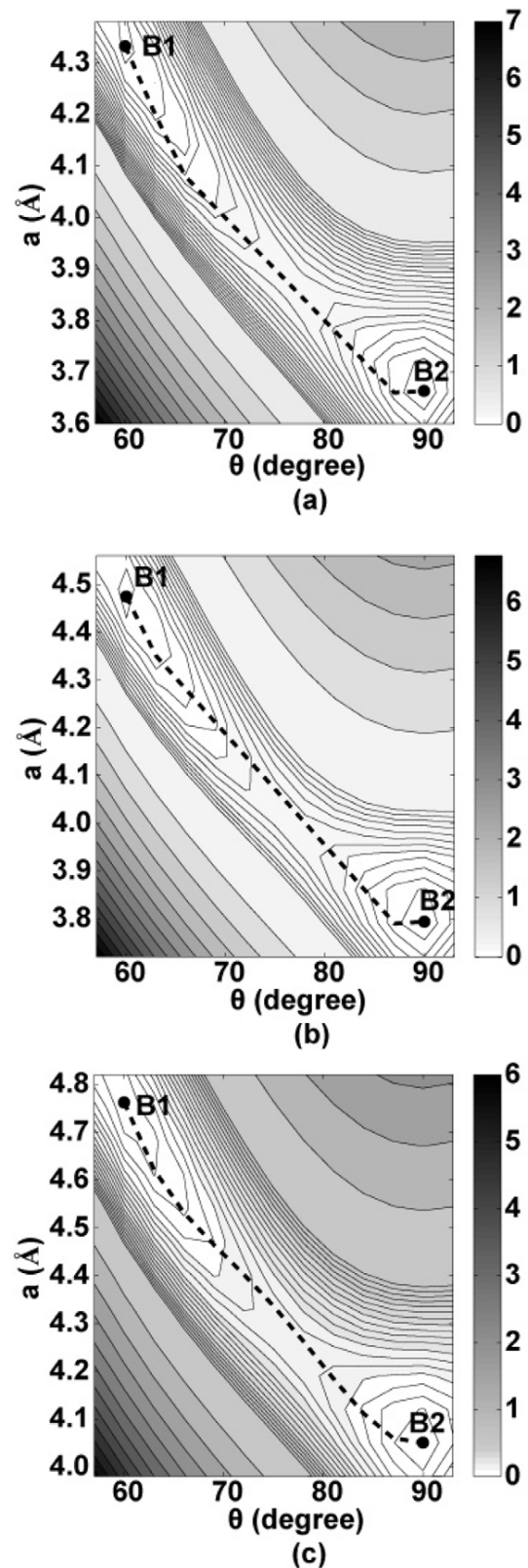


**Figure 4.** Contour plot of the computed enthalpy as a function of  $\theta$  and  $a$  of (a) BaS at 5.5 GPa, (b) BaSe at 3.4 GPa and (c) BaTe at 3.4 GPa for mechanism I. The scale bars indicate the enthalpy in eV. The dashed lines indicate the computed transition path from the B1 to the B2 structure. Coefficients to the polynomial fits governing the equations determining the paths are shown in table 2. The angle  $\theta$  and lattice constant  $a$  of the rhombohedral unit cell are defined in figure 1(a).

**Table 1.** Lattice constants,  $a$  (Å), at zero and transition pressures for the B1 and B2 structures of BaS, BaSe and BaTe. The transition pressure ( $P_t$ ) and percentage change in volume ( $\Delta V/V_{B1}$ ) as the phase changes from B1 to B2 along with the zero pressure bulk modulus  $B_0$  for the B1 and B2 structures also shown. Results from earlier work are given for comparison where available, with experimental data in parentheses and theoretical data in square brackets.

Material	$a$ (Å) B1	$a$ (Å) B1 at $P_t$	$a$ (Å) B2	$a$ (Å) B2 at $P_t$	$P_t$ (GPa)	$\Delta V/V_{B1}$ at $P_t$	$B_0$ (B1) (GPa)	$B_0$ (B2) (GPa)
BaS	6.316	6.139	3.768	3.670	5.473	14.54%	49.6	54.3
	(6.387 <sup>a</sup> )	(6.157 <sup>a</sup> )	[3.874 <sup>b</sup> ]	(3.693 <sup>a</sup> )	(6.5 <sup>a</sup> )	(13.68% <sup>a</sup> )	(55.1 <sup>g</sup> )	(21.4 <sup>g</sup> )
	[6.316 <sup>b</sup> ]				[6.51 <sup>b</sup> ]	[15.5% <sup>b</sup> ]	[53.32 <sup>b</sup> ]	[49.50 <sup>b</sup> ]
	[6.294 <sup>c</sup> ]				[6.025 <sup>c</sup> ]		[52.46 <sup>c</sup> ]	[60.84 <sup>c</sup> ]
	[6.407 <sup>d</sup> ]			[7.3 <sup>d</sup> ]				
BaSe	6.521	6.328	3.904	3.794	4.866	13.79%	42.5	47.9
	(6.593 <sup>e</sup> )		[3.874 <sup>b</sup> ]		(6.0 <sup>e</sup> )	(13.9% <sup>e</sup> )	(43.4 <sup>h</sup> )	(41.9 <sup>h</sup> )
	[6.511 <sup>b</sup> ]				[6.02 <sup>b</sup> ]	[14.6% <sup>b</sup> ]	[45.95 <sup>b</sup> ]	[49.50 <sup>b</sup> ]
	[6.508 <sup>c</sup> ]				[5.2 <sup>c</sup> ]		[45.41 <sup>c</sup> ]	[52.9 <sup>c</sup> ]
	[6.640 <sup>d</sup> ]							
BaTe	6.923	6.734	4.154	4.050	3.417	12.99%	34.1	38.0
	(7.005 <sup>f</sup> )		[4.122 <sup>b</sup> ]		(4.8 <sup>f</sup> )	(13.2% <sup>f</sup> )	(29.4 <sup>f</sup> )	(27.5 <sup>f</sup> )
	[6.920 <sup>b</sup> ]				[4.52 <sup>b</sup> ]	[14.1% <sup>b</sup> ]	[35.68 <sup>b</sup> ]	[40.04 <sup>b</sup> ]
	[6.978 <sup>c</sup> ]				[3.95 <sup>c</sup> ]		[33.75 <sup>c</sup> ]	[39.41 <sup>c</sup> ]
	[6.989 <sup>d</sup> ]							

<sup>a</sup> Reference [12]. <sup>b</sup> Reference [11]. <sup>c</sup> Reference [20]. <sup>d</sup> Reference [21]. <sup>e</sup> Reference [13]. <sup>f</sup> Reference [14]. <sup>g</sup> Reference [34]. <sup>h</sup> Reference [15].

**Table 2.** Coefficients ( $C_m$ ) of the cubic polynomial fits to the computed transition paths for the lattice constant  $a$  as a function of angle  $\theta$  in mechanism I, and lattice constants  $a$ ,  $b$  and  $c$  as a function of the internal parameter  $x$  in mechanism II of BaS, BaSe and BaTe. The equations used for fitting are:  $a$  (Å) =  $\sum_{m=0}^3 C_m \theta^m$  for mechanism I, while  $a$  (Å) =  $\sum_{m=0}^3 C_m x^m$ ,  $b$  (Å) =  $\sum_{m=0}^3 C_m x^m$  and  $c$  (Å) =  $\sum_{m=0}^3 C_m x^m$  for mechanism II. Note that the  $C_m$  coefficients have different values in each of the equations. The corresponding coefficient of determination ( $R^2$ ) fits, giving the quality of the fit, is shown in the last column. Values close to 1 in the last column signify the quality of the fit. The transition paths corresponding to these best fits are shown by the dashed lines in figures 4 and 5.

Material	Mechanism	Parameter	$C_3$	$C_2$	$C_1$	$C_0$	$R^2$
BaS	I	A	$-1.2262 \times 10^{-5}$	$3.1849 \times 10^{-3}$	$-2.9061 \times 10^{-1}$	$1.2939 \times 10^1$	0.994
		B	11.089	$-7.2777$	$-0.50539$	4.3506	0.994
	II	A	$-5.6161$	3.7126	1.2326	4.2948	0.982
		C	$-11.228$	6.7915	$-2.4688$	6.1496	0.991
BaSe	I	A	$4.2023 \times 10^{-6}$	$-6.9674 \times 10^{-4}$	$9.8855 \times 10^{-3}$	$5.4641 \times 10^0$	0.995
		B	13.961	$-9.7152$	$-0.018261$	4.4900	0.997
	II	A	$-4.1537$	3.8111	0.88618	4.4414	0.986
		C	$-26.608$	17.761	$-4.0371$	6.3401	0.957
BaTe	I	A	$-2.5658 \times 10^{-6}$	$8.7250 \times 10^{-4}$	$-1.1069 \times 10^{-1}$	$8.7929 \times 10^2$	0.994
		B	17.022	$-11.731$	0.18954	4.7705	0.997
	II	A	$-6.5722$	5.1451	0.99374	4.7318	0.989
		C	$-21.201$	13.439	$-3.3871$	6.7444	0.987

For mechanism II, the orthorhombic unit cell is determined by four variables, the three lattice constants ( $a$ ,  $b$  and  $c$ ) and the internal parameter  $x$ . The change of the three lattice constants ( $a$ ,  $b$  and  $c$ ) is not completely independent. It is found that an increase of the internal parameter  $x$  is always accompanied with decreases of the lattice constants  $a$  and  $c$ , and an increase of the lattice constant  $b$ . The two structural parameters  $x$  and  $c$ , which are used to visualize the PES, are represented by the abscissa and ordinate, respectively. On the transition pathway from the B1 to the B2 structure, the change of the internal parameter  $x$  is generally faster than the change of the lattice constant  $c$  before the saddle point, while the change of the lattice constant  $c$  is generally faster after the saddle point. Compared with mechanism I, the PES plots of mechanism II are smoother even though there is a steep and high energy elevation on the left bottom corner of each PES.

No other metastable phase, i.e. minimum, other than the B1 and B2 phases, is found on any of the PES plots. This indicates that there is no intermediate phase in this phase transition for both types of mechanisms, which is consistent with experimental observations for BaS [12–14].

The transition energy barriers of BaS at 0, 5.5 and 8.0 GPa, BaSe at 0, 4.9 and 8.0 GPa, and BaTe at 0, 3.4 and 5.5 GPa for both mechanisms are shown in table 3. From the corresponding PES plots, it is found that the transition state, whose structure exhibits the maximum enthalpy on the transition path, occurs early on the transition path for both mechanism I and mechanism II. Moreover, the energy barrier decreases for both mechanisms as the pressure increases, which suggests that the kinetics of the transition will proceed faster at higher pressure, consistent with experimental observations for BaS [12]. The energy barriers for a given

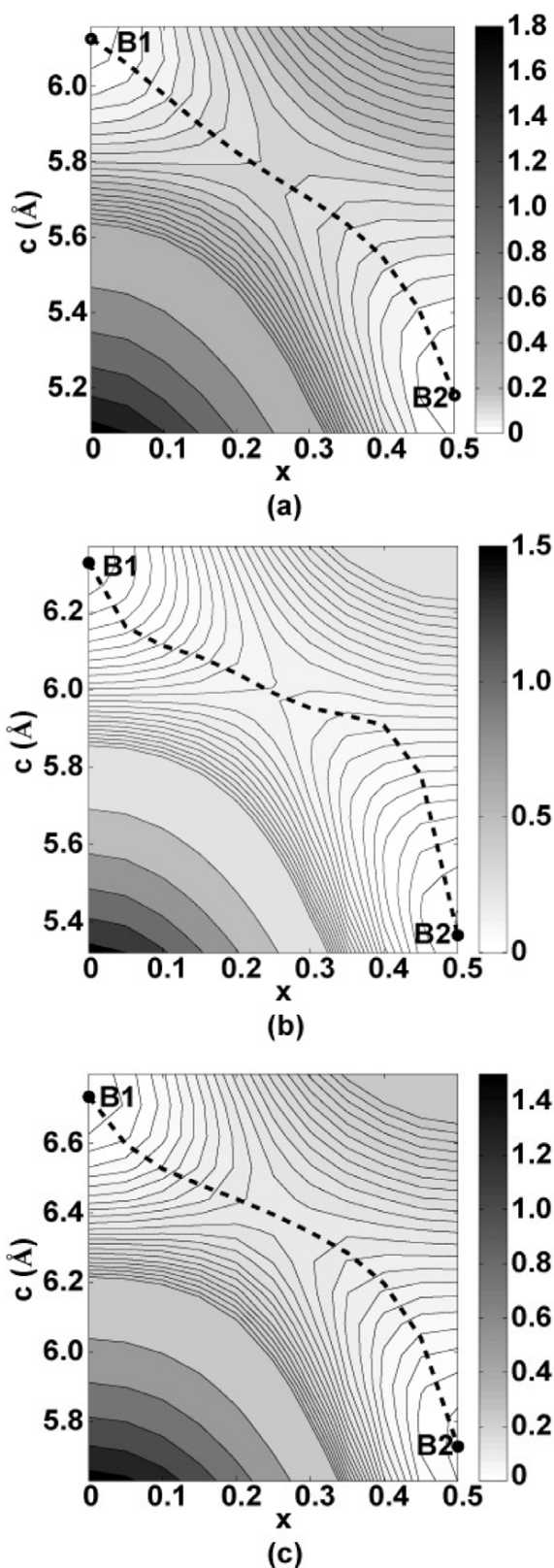


**Figure 5.** Contour plot of the computed enthalpy as a function of  $x$  and  $c$  of (a) BaS at 5.5 GPa, (b) BaSe at 3.4 GPa and (c) BaTe at 3.4 GPa for mechanism II. The scale bars indicate the enthalpy in eV. The dashed lines indicate the computed transition path from the B1 to the B2 structure. Coefficients to the polynomial fits governing the equations determining the paths are shown in table 2. The internal parameter  $x$  and lattice constant  $c$  of the orthorhombic cell are defined in figure 1(b).

**Table 3.** Energy barriers in eV/pair and  $\text{kJ mol}^{-1}$  (in parentheses) for the transition from B1 to B2 phase for BaS, BaSe and BaTe at three different pressures with mechanism I and mechanism II.

Material	Pressure (GPa)	Energy barrier (eV/pair ( $\text{kJ mol}^{-1}$ ))	
		Mechanism I	Mechanism II
BaS	0	0.35 (33.8)	0.32 (30.9)
	5.5	0.18 (17.4)	0.13 (12.5)
	8	0.12 (11.6)	0.08 (7.7)
BaSe	0	0.32 (30.9)	0.30 (28.9)
	4.9	0.16 (15.4)	0.13 (12.5)
BaTe	8	0.09 (8.7)	0.07 (6.8)
	0	0.28 (27.0)	0.25 (24.1)
	3.4	0.15 (14.5)	0.12 (11.6)
	5.5	0.10 (9.6)	0.08 (7.7)

compound at the same pressure for mechanism I are higher, by about 0.02 to 0.05 eV/pair ( $2\text{--}5 \text{ kJ mol}^{-1}$ ) than those for mechanism II. These small differences in energy per pair suggest that mechanism II is marginally favored over mechanism I during the phase transition from B1 to B2 for all BaX.

### 5.3. Symmetry and coordination

The phase transition leads to an eight-coordinated B2 structure from a six-coordinated B1 structure. Figure 6 gives a comparison between the coordination environments of sulfur atoms of BaS in the transition state at the transition pressure for both mechanism I and mechanism II. The four nearest neighbors on the (110) plane for mechanism I and the (002) plane for mechanism II form a rectangle, which is retained during the entire transition path. The sulfur atoms are located in the center of these rectangles. In mechanism I, the nearest and second nearest neighbors on the (110) plane enclose a parallelogram with the sulfur atom on its inversion center and the nearest neighbors on its shorter diagonal. In mechanism II, the nearest and second nearest neighbors on the (020) plane enclose a rectangle with the (020) plane as its mirror plane. For both mechanisms, the symmetry and coordination environments of Se and Te atoms in BaSe and BaTe, respectively, are similar to those of the S atom.

Due to the symmetry of the unit cell, the six nearest neighbors of the X atom in mechanism I are always equidistant, and this distance increases from the B1 to B2 structure. In contrast, as the transition proceeds, the two second nearest neighbors move closer to X until it finally has eight nearest neighbors in total in the B2 phase. In mechanism II, symmetry requirements are not as stringent on the nearest neighbor distances of the X atom. The distances to the X atom from the nearest neighbors in the (002) and (020) planes, defined as D1 and D2 respectively, are *not mandated* by symmetry to be equal. However, our analysis reveals that they are equal within the error bars associated with our computations along the transition path. As shown in figure 6, our calculations (with an error of  $\pm 0.02 \text{ \AA}$ ) reveal a D1 and D2 of 3.08 and 3.06  $\text{\AA}$  respectively for the transition state of BaS at 5.5 GPa, 3.18 and 3.16  $\text{\AA}$  for BaSe at 4.9 GPa and

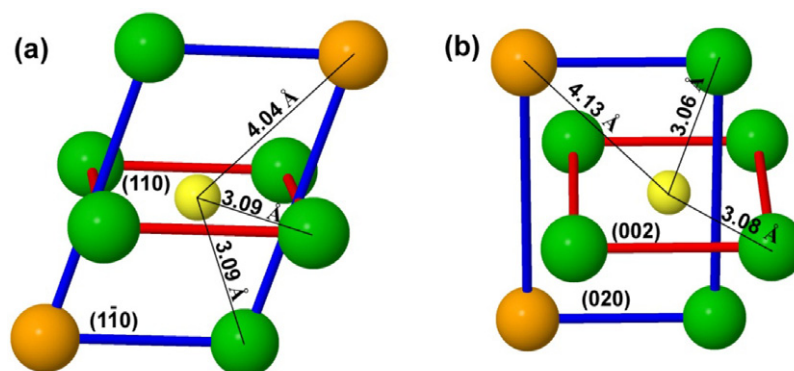


**Figure 6.** The nearest (green) and second nearest (orange) neighboring barium atoms of sulfur atoms in the transition state at 5.5 GPa of (a) mechanism I and (b) mechanism II. The Ba atoms in the (110) plane in (a) and the (002) plane in (b) form a rectangle, and the sulfur atoms in the (110) plane in (a) and the (002) plane in (b) are located on inversion centers and mirror planes, respectively.

3.40 and 3.39 Å for BaTe at 3.4 GPa. This was not analyzed in earlier experimental work [2] and may be tested upon further experimental investigation. Therefore, the major difference between mechanism I and mechanism II is the movement of the two planes adjacent to the (110) plane and the (002) plane respectively. The two planes in mechanism I move in opposite directions while the two planes in mechanism II move in the same direction.

## 6. Conclusions

In this paper, we have studied the pressure-induced B1 to B2 phase transition of BaX (X = S, Se and Te) for both the Buerger (I) and WTM (II) mechanisms at three different pressures by using first-principles calculations. By constructing energy hypersurfaces, we have proposed modeled transition paths and obtained the energy barriers of the phase transitions, which indicate that the WTM mechanism is marginally favored for the pressure-induced phase transition of all three BaX compounds. No intermediate state was found during the pressure-induced phase transition from the B1 to B2 phase for BaX. We discovered that the coordination number of the X atoms remains six throughout the transition as mandated by symmetry in mechanism I and despite any such mandate in mechanism II until the final B2 structure is reached.

## Acknowledgments

The authors would like thank the Ohio Supercomputer Center (OSC) for providing the computing resources. We thank the National Science Foundation (#DMR 1005911, #DMR 0705464, CNS 0855134 and CMMI 1234777) for funding this work.

## References

[1] Buerger M 1948 *Phase Transformations in Solids* ed R Smoluchowski, J E Mayer and W A Weyl (New York: Wiley) p 183

- [2] Watanabe M, Tokonami M and Morimoto N 1977 *Acta Crystallogr. A* **33** 294
- [3] Stokes H T and Hatch D M 2002 *Phys. Rev. B* **65** 144114
- [4] Onodera A, Kawano S, Nakai Y and Achiwa N 1992 *Physica B* **180** 279
- [5] Pendas A M, Luana V, Recio J M, Florez M, Francisco E, Blanco M A and Kantorovich L N 1994 *Phys. Rev. B* **49** 3066
- [6] Sims C E, Barrera G D, Allan N L and Mackrodt W C 1998 *Phys. Rev. B* **57** 11164
- [7] Catti M 2004 *J. Phys.: Condens. Matter* **16** 3909
- [8] Mota R C, Branicio P S and Rino J P 2006 *Europhys. Lett.* **76** 836
- [9] Toledano P, Knorr K, Ehm L and Depmeier W 2003 *Phys. Rev. B* **67** 144106
- [10] Stokes H T, Hatch D M, Dong J and Lewis J P 2004 *Phys. Rev. B* **69** 174111
- [11] Bouhemadou A, Khenata R, Zegrar F, Sahnoun M, Baltache H and Reshak A H 2006 *Comput. Mater. Sci.* **38** 263
- [12] Yamaoka S, Shimomura O, Nakazawa H and Fukunaga O 1980 *Solid State Commun.* **33** 87
- [13] Grzybowski T A and Ruoff A L 1983 *Phys. Rev. B* **27** 6502
- [14] Grzybowski T A and Ruoff A L 1984 *Phys. Rev. Lett.* **53** 489
- [15] Ruoff A L and Grzybowski T A 1985 *Solid State Physics Under Pressure* ed S Minomura (Tokyo: Terra Scientific)
- [16] Weir S T, Vohra Y K and Ruoff A L 1987 *Phys. Rev. B* **35** 874
- [17] Jha P K, Sakalle U K and Sanyal S P 1998 *J. Phys. Chem. Solids* **59** 1633
- [18] Durandurdu M 2010 *Chem. Phys.* **367** 80
- [19] Potzel O and Taubmann G 2011 *J. Solid State Chem.* **184** 1079
- [20] Kalpana G, Palanivel B and Rajagopalan M 1994 *Phys. Rev. B* **50** 12318
- [21] Lin G Q, Gong H and Wu P 2005 *Phys. Rev. B* **71** 085203
- [22] Zahn D and Leoni S 2004 *Phys. Rev. Lett.* **92** 250201
- [23] Zahn D, Hochrein O and Leoni S 2005 *Phys. Rev. B* **72** 094106
- [24] Kresse G 1993 *Ab initio* molekular dynamik für flüssige metalle *PhD Dissertation* Technische Universität Wien
- [25] Kresse G and Hafner J 1993 *Phys. Rev. B* **47** 558
- [26] Kresse G and Furthmüller J 1996 *Comput. Mater. Sci.* **6** 15
- [27] Kresse G and Furthmüller J 1996 *Phys. Rev. B* **54** 11169
- [28] Hohenberg P and Kohn W 1964 *Phys. Rev. B* **136** 864
- [29] Kohn W and Sham L J 1965 *Phys. Rev. A* **140** 1133
- [30] Vanderbilt D 1990 *Phys. Rev. B* **41** 7892
- [31] Kresse G and Hafner J 1994 *J. Phys.: Condens. Matter* **6** 8245
- [32] Monkhorst H J and Pack J D 1976 *Phys. Rev. B* **13** 5188
- [33] Cai J and Chen N X 2007 *J. Phys.: Condens. Matter* **19** 266207
- [34] Weir S T, Vohra Y K and Ruoff A L 1986 *Phys. Rev. B* **33** 4221